Gunnarsson, David; Tuorila, Jani; Paila, Antti; Sarkar, Jayanta; Thuneberg, Erkki; Makhlin, Yuriy; Hakonen, Pertti

Vibronic spectroscopy of an artificial molecule

Published in:
Physical Review Letters

DOI:
10.1103/PhysRevLett.101.256806

Published: 01/01/2008

Document Version
Publisher's PDF, also known as Version of record

Vibronic Spectroscopy of an Artificial Molecule

David Gunnarsson,[1] Jani Tuorila,[2] Antti Paila,[1] Jayanta Sarkar,[1] Erkki Thuneberg,[2] Yuriy Makhlin,[3] and Pertti Hakonen[1]

[1]*Low Temperature Laboratory, Helsinki University of Technology, FI-02015 HUT, Finland*
[2]*Department of Physical Sciences, University of Oulu, FI-90014, Finland*
[3]*Landau Institute for Theoretical Physics, Kosygin Street 2, 119334 Moscow, Russia*

(Received 15 August 2008; published 19 December 2008)

We have performed microwave reflection experiments on a charge-phase qubit coupled to an LC oscillator. We find that the system behaves like an artificial molecule showing vibronic sideband transitions. The reflected signal is determined by a combination of the Franck-Condon principle and resolved-sideband cooling or heating of the oscillator.

DOI: 10.1103/PhysRevLett.101.256806 PACS numbers: 85.35.Gv, 73.23.Hk, 74.50.+r

With advanced fabrication techniques, it is possible to make nanoscale electronic structures that have discrete energy levels. Such structures are called artificial atoms because of analogy with true atoms. Examples of such atoms are quantum dots in semiconductor heterostructures [1,2] and Josephson-junction qubits [3–7]. It is also possible to have artificial atoms interacting with each other. This is an artificial molecule in the sense that the electronic states are analogous to the ones in a molecule [8]. In this Letter, we present a different type of artificial molecule that, in addition to electronic states, also includes the analog of nuclear vibrations in a diatomic molecule. In our case, the electronic states of the molecule are represented by a Josephson-junction qubit, and the nuclear separation corresponds to the magnetic flux in a loop containing the qubit and an LC oscillator.

The potentials in our artificial molecule are illustrated in Fig. 1. The two states of the qubit correspond to two electronic states in a molecule. For both, there are several vibrational states. Associated with a transition between the electronic states there often is a simultaneous change in the vibrational state, and such transitions are called vibronic. The intensity of vibronic transitions is governed by the Franck-Condon principle [9,10]. In its classical form, the principle says that transitions are possible between vibrational states whose trajectories intersect in phase space [11] and they are most intense between states having coincident turning points. We have made spectroscopic studies of the artificial molecule. By a low-frequency drive we excite the vibrations, and by a simultaneous high-frequency drive we can induce the vibronic transitions. We find that the reflected low-frequency wave is determined by the Franck-Condon principle combined with resolved-sideband cooling or heating of the vibrations [12].

A large number of experiments could be interpreted using the molecular analogy, including qubits coupled to oscillators [13–22] and qubits driven by an intense field [23–27]. The analogy is particularly apt for our case because there is clear separation of the electronic and vibrational energy scales, we drive at two frequencies, and the parameters of the molecule can be tuned in a wide range.

The circuit of our artificial molecule is shown in Fig. 2. The heart of it is a single-Cooper-pair transistor (SCPT). It consists of a 2 μm long Al island surrounded by two Josephson junctions with coupling energies $E_{J1} \approx E_{J2}$, as well as capacitances C_1 and C_2, respectively. The SCPT is fabricated using the standard procedure of two angle evaporation [28]. The SCPT is coupled in parallel to an LC oscillator. The inductor of the oscillator is formed by a superconducting on-chip microstrip loop of length 300 μm giving $L = 169$ pH. The capacitance $C = 196.2$ pF is formed by two parallel plate capacitors acting in series. These are made by patterning two 1.3×1.3 mm^2 Al plates on the Si_3N_4/Nb/Si sandwich substrate. The bottom plate of the capacitor is formed by a 150 nm thick niobium back gate under the dielectric Si_3N_4 layer, whose thickness is around 300 nm. The data were taken at the base temperature of the refrigerator $T = 25$ mK. In addition to several stages of band pass filtering by Minicircuits VLX-series filters, we used two circulators at 25 mK to prevent

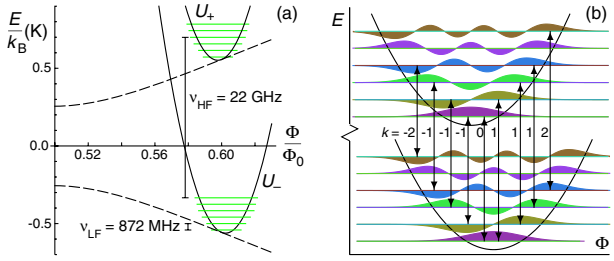

FIG. 1 (color online). The potential energy and energy eigenstates in the artificial molecule (1). (a) The total potentials $U_\pm$ (solid curves) are formed as a sum of qubit energy (dashed line) and a harmonic vibrational potential. The six lowest energy eigenstates are shown for both electronic states. The bars represent the energy differences $\Delta E = h\nu$ corresponding to the drives of low- and high-frequency, ν_{LF} and ν_{HF}, respectively. The parameters are for the bias point $(\Phi_b, n_g) = (0.60\Phi_0, 1.16)$. (b) A close-up at the lowest eigenstates together with wave functions (shaded areas). The strongest transitions according to the Franck-Condon principle are shown by arrows and are labeled by the change of vibrational quanta k.

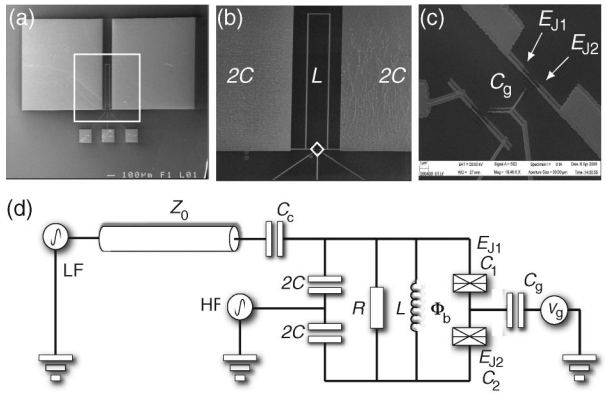

FIG. 2. Scanning electron microscopy micrographs and circuit diagram of the artificial molecule. (a) General view showing top electrodes of the oscillator capacitors (2 large pads) with capacitances $2C$ each. (b) Enlargement of the white square area in (a) showing the 300 μm-long microstrip loop that forms the inductance L of the oscillator. (c) Magnification of the white diamond in (b) showing the SCPT formed by two Josephson junctions with coupling energies E_{J1} and E_{J2} and the gate electrode. Also visible is a reference SCPT (lower left) which enables one to estimate the resistances of the junctions in the sample. (d) The circuit diagram shows the SCPT and the LC oscillator connected in parallel. The resistance $R = 2.8$ kΩ represents the ac dissipation of the capacitors as well as of other parts of the circuit. The artificial molecule is biased by a gate voltage V_g and an external magnetic flux Φ_b. The low-frequency drive (LF) is applied through a $Z_0 = 50\ \Omega$ transmission line via a lumped-element coupling capacitor $C_c = 7$ pF, which is wire bonded to the top plate of one of the $2C$ capacitors. The high-frequency drive (HF) is applied through a separate $Z_0 = 50\ \Omega$ transmission line and is wire bonded to the back gate of the sample. The back gate is in turn wire bonded to the ground. The inductances of the bond wires give voltage division and thus a finite V_{HF} over the SCPT.

the backaction noise of our cryogenic low-noise amplifier from reaching the qubit.

The artificial molecule has two parameters that can be adjusted in the experiment. The dc gate voltage V_g changes the gate charge $en_g = C_g V_g$, which controls the tunneling of Cooper pairs to and from the island. The other parameter is the magnetic flux bias Φ_b through the inductor loop caused by an external magnetic field. This controls the Josephson coupling E_J of the island as the flux shifts the relative phases of the two junctions and leads to complete suppression at $\Phi_b = \Phi_0/2$ in a symmetric SCPT. Here $\Phi_0 = h/2e$ is the flux quantum. The properties of the SCPT can be calculated in detail using Mathieu functions [29] and including the asymmetry of the junctions. Instead of the general analysis, we present here a simplified treatment that is still sufficient to understand the main properties of the circuit. In the charge limit $E_J \ll E_c = e^2/(C_1 + C_2 + C_g)$, the SCPT forms a qubit where only two charge states are of importance. They correspond to having one Cooper pair more or less on the island. In this basis the Hamiltonian of the SCPT is $H_q = \frac{1}{2} \times [\sigma_z E_{\mathrm{el}} - \sigma_x E_{J0} \cos(\pi\Phi/\Phi_0)]$, where $E_{J0} = E_{J1} + E_{J2}$, $E_{\mathrm{el}} = 4E_c(1 - n_g)$, and σ_i are Pauli matrices. Diagonalizing the Hamiltonian gives two eigenvalues $E^q_{\pm} = \pm\frac{1}{2}\sqrt{E^2_{\mathrm{el}} + E^2_{J0}\cos^2(\pi\Phi/\Phi_0)}$, which correspond to two "electronic" states of the artificial molecule.

The LC circuit forms a harmonic oscillator, whose Hamiltonian $H_v = q^2/2C + (\Phi - \Phi_b)^2/2L$. Taking the flux Φ as a generalized coordinate, the charge q on the capacitor is the corresponding canonical momentum. The total Hamiltonian is $H_q + H_v$. Assuming that the vibrations are slow, we can use the adiabatic energies $E^q_{\pm}$ for the qubit. Thus the total potential energy U of the "molecule" is

$$U_{\pm}(\Phi) = \pm\frac{1}{2}\sqrt{E^2_{\mathrm{el}} + E^2_{J0}\cos^2\frac{\pi\Phi}{\Phi_0}} + \frac{(\Phi - \Phi_b)^2}{2L}. \quad (1)$$

This is plotted in Fig. 1 using parameters appropriate for our circuit. We see that the electronic and vibrational degrees of freedom are coupled as both depend on the flux Φ. The LC oscillator potential vanishes at the bias point Φ_b, but, because of opposite slopes of the qubit energies, the minima of the total potentials are shifted in opposite directions [23,27]. Because of the different curvatures of the qubit potentials, the vibrational resonance frequencies $\nu_{\pm}$ in the two electronic states are different [15,17,18].

The measurement is done by sending in a low-frequency signal typically at the frequency $\nu_{\mathrm{LF}} = 872$ MHz. This is slightly below the LC oscillator resonance frequency $\nu_0 = 874$ MHz. The reflected signal was continuously monitored using a network analyzer set to detect magnitude and phase in a band width of 10 kHz. Being close to resonance, the reflected signal depends essentially on the vibrational frequency determined by the curvature of the qubit energy. As this varies as a function of the bias point (Φ_b, n_g), one can use the data on the electronic ground state to fit the parameters of the qubit. We find $E_c/k_B = 0.8$ K, $E_{J0}/k_B = 3.2$ K, and the asymmetry parameter $d = (E_{J1} - E_{J2})/(E_{J1} + E_{J2}) = 0.04$.

In order to study the vibronic transitions, a second drive operating at a high frequency ν_{HF} was applied. Figure 3 shows the results for $\nu_{\mathrm{HF}} = 22$ GHz. The reflection coefficient is plotted over the (Φ_b, n_g) bias plane for two different low-frequency power levels P_{LF}. The main observation is the fringes (yellowish or light blue in the color figure). There is one fringe starting at $(\Phi_b, n_g) = (\Phi_0/2, 1.32)$. With increasing Φ_b, more fringes appear as they simultaneously are curving down. One sees that the fringes form concentric and equally spaced ellipses around the point $(\Phi_0/2, 1)$. We associate the fringe denoted by the dashed line with a pure electronic transition and the other fringes with vibronic transitions. The concentric structure can be understood because in this region the energies are to a good

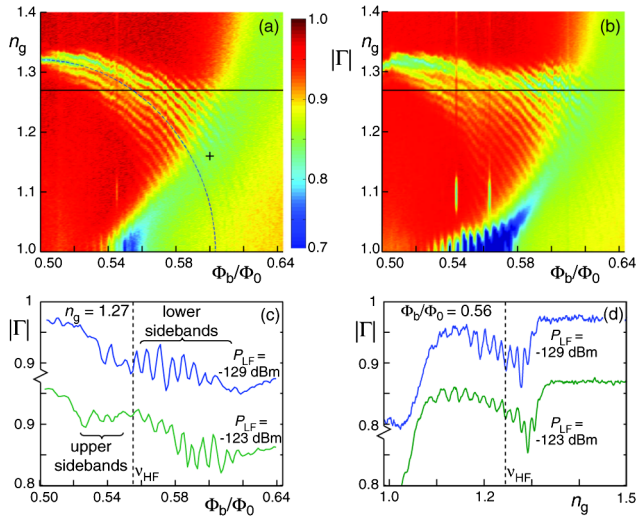

FIG. 3 (color online). Measured spectra of the artificial molecule. (a) The absolute value of the reflection coefficient $\Gamma = V_{\rm out}/V_{\rm in}$ as a function of the bias point (Φ_b, n_g). The color bar gives the scale for $|\Gamma|$. The dashed arch indicates the pure electronic transition at $\Delta E/h = \nu_{\rm HF} = 22$ GHz. The cross denotes the bias point of Fig. 1 where $k = -2$. The applied low-frequency power $P_{\rm LF} = -129$ dBm, and the high-frequency flux amplitude over the SCPT is approximately $8 \times 10^{-4}\Phi_0$. (b) The same as (a) but at higher $P_{\rm LF} = -123$ dBm. (c) A cut along $n_g = 1.27$ as indicated by the horizontal lines in (a) and (b). (d) A cut along $\Phi_b = 0.56\Phi_0$.

accuracy given by Eq. (1) and, moreover, $\cos(\pi\Phi/\Phi_0) \approx -\pi(\Phi/\Phi_0 - \frac{1}{2})$. This means that the difference in the qubit energies increases linearly with the distance in the vicinity of the degeneracy point $(\Phi_0/2, 1)$. In other words, the qubit bands have a conical shape, and the fringes correspond to approximately constant energies. The radii of the fringes are in agreement with the imposed frequencies and the parameters of the qubit $\nu_{\rm HF} = (E^q_+ - E^q_-)/h + k\nu_0$, with integer k. We call the vibronic transitions inside of the dashed line upper (or blue) sidebands and outside lower (or red) sidebands, as they are relative to the pure electronic transition at the same bias point ($k > 0$ and $k < 0$, respectively).

The visibility of the fringes is consistent with the Franck-Condon principle illustrated in Fig. 1. In particular, at a half flux quantum ($\Phi_b = \Phi_0/2$) only the pure electronic transition is visible. This is to be expected, since the minima of the potentials $U_\pm$ occur at the same Φ and thus only diagonal matrix elements in the vibrational states are nonzero. For increasing flux the potential minima get shifted, which allows vibronic transitions. The fringes appear in a crescent-shaped region, i.e., in a stripe that is centered at the basic fringe (dashed line) and whose width grows with Φ_b (together with the shift of the minima of U_- and U_+). It is just in this region that the classical trajectories of the oscillators intersect and lead to nonvanishing transition matrix elements. The boundary of this region corresponds to trajectories touching each other at coincident extrema $\Phi^{\rm ext}_+ = \Phi^{\rm ext}_-$ in the two electronic states. Equivalently, for the bias points at the boundary, the oscillation just reaches the locus of pure electronic transitions (dashed line in Fig. 3). This allows one to determine the oscillation amplitude corresponding to a given drive power $P_{\rm LF}$.

For further analysis of the fringes, we need to look more closely at the measurement details. In contrast to experiments with real molecules, we do not detect directly the absorption or emission of the vibronic quanta. Instead, we measure the reflection of the low-frequency wave. Two effects on the signal can be separated. (i) The first one is a usual resonance absorption taking place when the wave frequency is close to the vibrational frequency $\nu_\pm$. This is different in the upper and lower qubit states, but the measurements are consistent with a "motional averaging" picture that there is only one Lorentzian line whose resonance frequency is an average of ν_- and ν_+ weighted by the occupations of the qubit states. This is essential for the visibility of the fringes near $\Phi_b \approx \Phi_0/2$ as both the upper and lower state frequencies would be far away to give any noticeable absorption. (ii) The second effect is a damping or amplification effect that is similar to resolved-sideband cooling in optics [12]. The same effect has been discussed also in Josephson qubits [30] and has been seen for the first vibronic transitions [22]. Consider the lower sideband fringes in Fig. 3. The absorption of a high-frequency quantum brings the system to a lower vibrational state. When the electronic part of the excitation relaxes by another route, this leads to damping of the vibrations. In a steady state, this leads to increased absorption as the low-frequency drive has to supply the missing vibrational quanta. Conversely, in the case of an upper sideband, the absorption of a high-frequency quantum produces extra vibrational quanta leading to amplification of the oscilla-

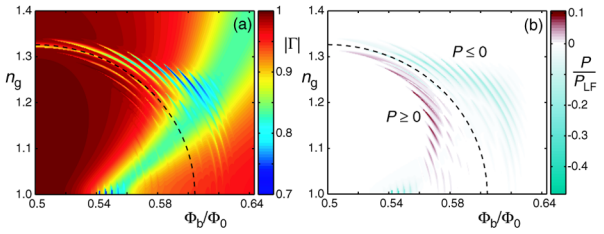

FIG. 4 (color online). Simulated properties of the artificial molecule. (a) The reflection amplitude $|\Gamma|$ calculated as a function of the bias point in the flux-charge plane. The parameters correspond to the measurement plotted in Fig. 3(a). (b) The energy flow from the qubit to the resonator showing damping for lower sideband transitions (blue) and amplification for the upper sideband transitions (red). The power unit is $P_{\rm LF} = -129$ dBm. The simulation uses cone approximation mentioned in the text as the difference to full Mathieu bands is small. The parameter values are given in the text including the asymmetry d, $T_1 = 40$ ns, and $T_2 = 2$ ns.

tion. This could lead to a low-frequency reflection coefficient exceeding unity and even to lasing [31]. In our system the losses in the vibrations cause us to see this only as a decrease in the absorption.

The damping or amplification effect of the high-frequency drive provides a natural explanation for the asymmetry of the upper and lower sideband fringes. In order to study this quantitatively, we have made numerical simulations using Bloch equations for the qubit and coupled to classical equations of the circuit. The simulated reflection amplitude $|\Gamma|$ is shown in Fig. 4(a). Figure 4(b) shows the energy flow from the qubit to the oscillator. This is defined as $P_{\mathrm{LF,R}}$-$P_{\mathrm{LF,A}}$, the low-frequency (LF) dissipation in the oscillator resistance minus the absorption from the LF drive in the steady state. We see that this is negative for lower sidebands and positive for upper sidebands, in accordance with the expectation. Thus we see the resolved-sideband cooling and heating effect of the vibronic transitions. With a different measurement method, not driving the object to be cooled, one should get damping of thermal fluctuations.

We comment on some additional features of the spectra in Fig. 3. There is a broad feature starting around $(0.54\Phi_0, 1)$ and shifting to larger Φ_b with increasing n_g. This is the line where the vibrations in the lower electronic state are in resonance with the low-frequency excitation $\nu_- = \nu_{\mathrm{LF}}$. This resonance is present also in the absence of microwave excitation and was used to fit the parameters of the qubit. On the side of smaller Φ_b, the vibronic transitions are well visible as increased absorption because of motional averaging since $\nu_- < \nu_{\mathrm{LF}} < \nu_+$. On the opposite side, ν_- is shifted above ν_{LF} and the fringes are less clear. There are resonances also around $(0.55\Phi_0, 1)$. They also occur in the absence of a high-frequency drive. They are caused by Landau-Zener tunneling at the point $(\Phi_0/2, 1)$, where the electronic energy difference is at minimum [25,26].

In conclusion, we demonstrated that our Josephson qubit coupled to an LC oscillator behaves like a tunable diatomic molecule, where the spectral weights of transitions obey the Franck-Condon principle. The vibronic transitions can be used for resolved-sideband cooling, and we see damping of the oscillations up to sidebands of order 10.

Fruitful discussions with M. Devoret, S. Girvin, T. Heikkilä, F. Hekking, T. Lehtinen, M. Paalanen, M. Sillanpää, and M. Silveri are gratefully acknowledged. This work was financially supported by the Academy of Finland, the National Technology Agency, the Finnish Cultural Foundation, the Magnus Ehrnrooth Foundation, EU-INTAS 05-10000008-7923, and EC-funded ULTI Project (Contract No. RITA-CT-2003-505313).

[1] M. Kastner, Phys. Today **46**, No. 1, 24 (1993).
[2] R. C. Ashoori, Nature (London) **379**, 413 (1996).
[3] Y. Nakamura, C. D. Chen, and J. S. Tsai, Phys. Rev. Lett. **79**, 2328 (1997).
[4] D. J. Flees, S. Han, and J. E. Lukens, Phys. Rev. Lett. **78**, 4817 (1997).
[5] V. Bouchiat, D. Vion, P. Joyez, D. Esteve, and M. H. Devoret, Phys. Scr. **T76**, 165 (1998).
[6] Y. Nakamura, Yu. A. Pashkin, and J. S. Tsai, Nature (London) **398**, 786 (1999).
[7] C. H. van der Wal *et al.*, Science **290**, 773 (2000).
[8] T. H. Oosterkamp *et al.*, Nature (London) **395**, 873 (1998).
[9] J. Franck, Trans. Faraday Soc. **21**, 536 (1926).
[10] E. Condon, Phys. Rev. **28**, 1182 (1926).
[11] W. P. Schleich, *Quantum Optics in Phase Space* (Wiley, Berlin, 2001).
[12] D. J. Wineland and W. M. Itano, Phys. Rev. A **20**, 1521 (1979).
[13] E. Il'ichev *et al.*, Phys. Rev. Lett. **91**, 097906 (2003).
[14] I. Chiorescu, P. Bertet, K. Semba, Y. Nakamura, C. J. P. M. Harmans, and J. E. Mooij, Nature (London) **431**, 159 (2004).
[15] A. Wallraff *et al.*, Nature (London) **431**, 162 (2004).
[16] A. Lupascu *et al.*, Phys. Rev. Lett. **93**, 177006 (2004).
[17] T. Duty *et al.*, Phys. Rev. Lett. **95**, 206807 (2005).
[18] M. A. Sillanpää *et al.*, Phys. Rev. Lett. **95**, 206806 (2005).
[19] J. Johansson *et al.*, Phys. Rev. Lett. **96**, 127006 (2006).
[20] D. Schuster *et al.*, Nature (London) **445**, 515 (2007).
[21] A. Wallraff *et al.*, Phys. Rev. Lett. **99**, 050501 (2007).
[22] M. Grajcar *et al.*, Nature Phys. **4**, 612 (2008).
[23] Y. Nakamura, Yu. A. Pashkin, and J. S. Tsai, Phys. Rev. Lett. **87**, 246601 (2001).
[24] S. Saito *et al.*, Phys. Rev. Lett. **93**, 037001 (2004).
[25] W. Oliver, Y. Yu, J. Lee, K. Berggren, L. Levitov, and T. Orlando, Science **310**, 1653 (2005).
[26] M. Sillanpää, T. Lehtinen, A. Paila, Yu. Makhlin, and P. Hakonen, Phys. Rev. Lett. **96**, 187002 (2006).
[27] C. M. Wilson *et al.*, Phys. Rev. Lett. **98**, 257003 (2007).
[28] T. A. Fulton and G. J. Dolan, Phys. Rev. Lett. **59**, 109 (1987).
[29] D. V. Averin, A. B. Zorin, and K. K. Likharev, Sov. Phys. JETP **61**, 407 (1985).
[30] I. Martin, A. Shnirman, L. Tian, and P. Zoller, Phys. Rev. B **69**, 125339 (2004).
[31] O. Astafiev *et al.*, Nature (London) **449**, 588 (2007).